Max-Planck-Institut
für Polymerforschung
Max Planck Institute
for Polymer Research

Direct Observation of Gas Meniscus Formation on a Superhydrophobic Surface

Mimmi Eriksson, Mikko Tuominen, Mikael Järn, Per M. Claesson, Viveca Wallqvist, Hans-Jürgen Butt, Doris Vollmer, Michael Kappl, Joachim Schoelkopf, Patrick Gane, Hannu Teisala, and Agne Swerin

Direct Observation of Gas Meniscus Formation on a Superhydrophobic Surface

Mimmi Eriksson [†*], Mikko Tuominen [†], Mikael Järn [†], Per M. Claesson [†‡], Viveca Wallqvist [†], Hans-Jürgen Butt [§], Doris Vollmer [§], Michael Kappl [§], Joachim Schoelkopf [∥], Patrick Gane [∥⊥], Hannu Teisala [§*] and Agne Swerin [†‡]

[†] RISE Research Institutes of Sweden, Bioscience and Materials – Surface, Process and Formulation, SE-114 86 Stockholm, Sweden
[‡] KTH Royal Institute of Technology, School of Engineering Sciences in Chemistry, Biotechnology and Health, Department of Chemistry, Division of Surface and Corrosion Science, SE-100 44 Stockholm, Sweden
[§] Max Planck Institute for Polymer Research, Department of Physics at Interfaces, Ackermannweg 10, DE-55128 Mainz, Germany
[∥] Omya International AG, CH-4665 Oftringen, Switzerland
[⊥] Aalto University, School of Chemical Engineering, Department of Bioproducts and Biosystems, FI-00076 Aalto, Espoo, Finland

*Corresponding authors: mimmi.eriksson@ri.se, teisala@mpip-mainz.mpg.de

ABSTRACT

The formation of a bridging gas meniscus *via* cavitation or nanobubbles is considered the most likely origin of the submicrometer long-range attractive forces measured between hydrophobic surfaces in aqueous solution. However, the dynamics of the formation and evolution of the gas meniscus is still under debate, and in particular in the presence of a thin air layer on a superhydrophobic surface. On superhydrophobic surfaces the range can even exceed 10 µm. Here, we report microscopic images of the formation and growth of a gas meniscus during force measurements between a superhydrophobic surface and a hydrophobic microsphere immersed in water. This is achieved by combining laser scanning confocal microscopy and colloidal probe atomic force microscopy. The configuration allows determination of the volume and shape of the meniscus, together with direct calculation of the Young-Laplace capillary pressure. The long-range attractive interactions acting on separation are due to meniscus formation and volume growth as air is transported from the surface layer.

KEYWORDS superhydrophobicity, wetting, laser scanning confocal microscopy, AFM colloidal probe, capillary forces.

Interactions between hydrophobic surfaces in aqueous solution have intrigued scientists for over 30 years,[1] and the formation of a bridging gas meniscus *via* vaporization of the surrounding liquid (*i.e.* cavitation) or nanobubbles[2] has become the most widely accepted mechanism behind the long-range attraction.[3-13] The formation of gaseous menisci in water between smooth hydrophobized surfaces has been observed with optical microscopy[14] and by using multiple-beam interferometry.[15] However, due to lack of time and space resolved data of sufficient resolution, the development of the meniscus volume and the shape of the interface between the gas phase and the liquid remain unclear. Furthermore, it is unclear how a gas meniscus evolves in the presence of a pre-existing air layer as characteristic for superhydrophobic surfaces.

A surface is typically regarded as superhydrophobic if it displays a water contact angle above 150° and a low roll-off angle (<5-10°). This requires a combination of low surface energy and micro- and nanoscale surface structures, *e.g.* as observed on the lotus leaf.[16-17] A liquid droplet resting on a rough hydrophobic surface is often described by two different basic wetting models, the Wenzel[18] and the Cassie-Baxter[19] states, even though intermediate or mixed states are also found.[20-21] In the Wenzel state, the liquid penetrates the depressions and fully wets the surface structure. In contrast, in the Cassie-Baxter state the droplet is suspended on top of the surface features with pockets of air trapped underneath.

Forces acting between rough hydrophobic and superhydrophobic surfaces in aqueous solution display long-range attractive interactions. The range exceeds those between smooth surfaces.[22-24] In addition, the shape of the force curves measured on separation is often found to be inconsistent with the presence of a gaseous meniscus with constant volume. Instead, an increase in the meniscus volume during separation caused by transport of gas from pockets trapped in the surface features has been suggested as a possible cause.[23-25] However, a clear understanding of these dynamic events is missing due to the lack of space and time resolved data.

Laser scanning confocal microscopy, in short, confocal microscopy, allows observations of the local wetting properties on rough surfaces in three dimensions with a resolution better than 1 µm.[26] It provides detailed information on static and dynamic aspects of the three-phase contact lines and wetting behavior of superhydrophobic surfaces.[27-30]

Here, we relate the forces measured between a hydrophobic microsphere and a superhydrophobic surface immersed in water with images of formation and evolution of gaseous menisci. This allows us to extract meniscus volume and shape as well as the wetted contact area and determine quantitatively the resulting Young-Laplace capillary pressures. We find that the meniscus volume grows due to transport of air from the layer at the superhydrophobic surface driven by the under-pressure in the meniscus.

RESULTS AND DISCUSSION

Superhydrophobic surfaces were prepared by dip coating cover glasses in a formulation containing silica nanoparticles. After gas phase silanization with 1H,1H,2H,2H-perfluorooctyltrietoxysilane, the coated samples displayed a macroscopic water contact angle of $\theta = 155 \pm 1°$ ($\theta_{adv} = 159 \pm 1°$, $\theta_{rec} = 147 \pm 5°$). A 5 µL water droplet rolled off when tilting the surface by 5 ±3°. The average

arithmetic (R_a) and root mean square roughness (R_q) were calculated from a 10×10 µm^2 atomic force microscopy (AFM) topography image (Figure 1a) to 95 nm and 123 nm, respectively. By gently scraping off the coating with a scalpel, its thickness was determined with AFM to 1-1.5 µm. A spherical glass particle with radius $R = 18.8$ µm was attached to a tipless cantilever (spring constant $k_z = 20$ N m^{-1}) and hydrophobized by gas phase silanization. The hydrophobic particle had a rather high surface roughness with $R_a = 39$ nm and $R_q = 49$ nm on a 5×5 µm^2 area (Figure S1, Supporting Information).
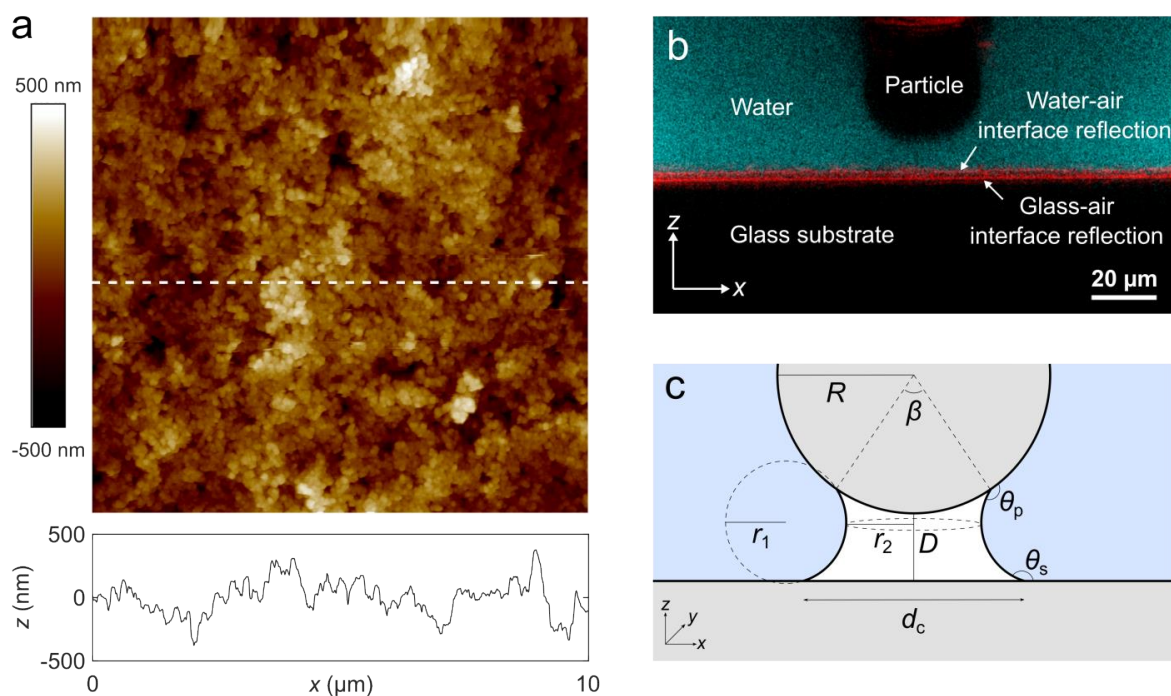

Figure 1. (a) AFM topographical image (10×10 µm^2) of the superhydrophobic surface and height profile along the horizontal dashed line in the center of the image. The surface chemistry of such a superhydrophobic surface was analyzed with X-ray photoelectron spectroscopy in a previous study,[35] showing a C/F ratio of 0.6 ±0.1 and a CF$_2$/CF$_3$ ratio of 5.1 ±0.3. (b) Confocal microscopy image with the light reflected from the interfaces in red and water with fluorescent dye in cyan. (c) Illustration of a gas meniscus between the hydrophobic particle (radius R) and the superhydrophobic surface at separation distance D, with the meniscus base diameter (d_c), the angle defining the de-wetted area on the hydrophobic particle (β), the microscopic contact angles at the liquid-gas interface of the particle (θ_p) and superhydrophobic surface (θ_s), and the two radii of the principal curvature of the liquid-gas interface (r_1 and r_2).

The force between the hydrophobic particle and the superhydrophobic surface in water was measured with colloidal probe AFM using a constant driving speed of 0.2 µm s^{-1} during approach and retraction. Simultaneously, a specially designed inverted confocal microscope[31-32] was used

3

for imaging. The aqueous phase was visualized by adding a low concentration (10 mg L^{-1}) of the hydrophilic fluorescent dye Atto 488 (Figure S2, Supporting Information). Vertical slices through the center of the hydrophobic particle were recorded at an acquisition rate of 1 frame s^{-1}. The fluorescence from the dyed water and the reflected light from the interfaces were detected simultaneously (Figure S3, Supporting Information) and combined into a composite image (Figure 1b). Two red lines close to the superhydrophobic surface arise from light reflected from the water-gas and glass-gas interfaces. The reflections demonstrate the presence of an air layer separating the coated glass substrate from the aqueous phase consistent with a Cassie-Baxter wetting state. The air layer was roughly 1-2 µm thick, and it was found to be stable throughout force measurements (Figure 2).
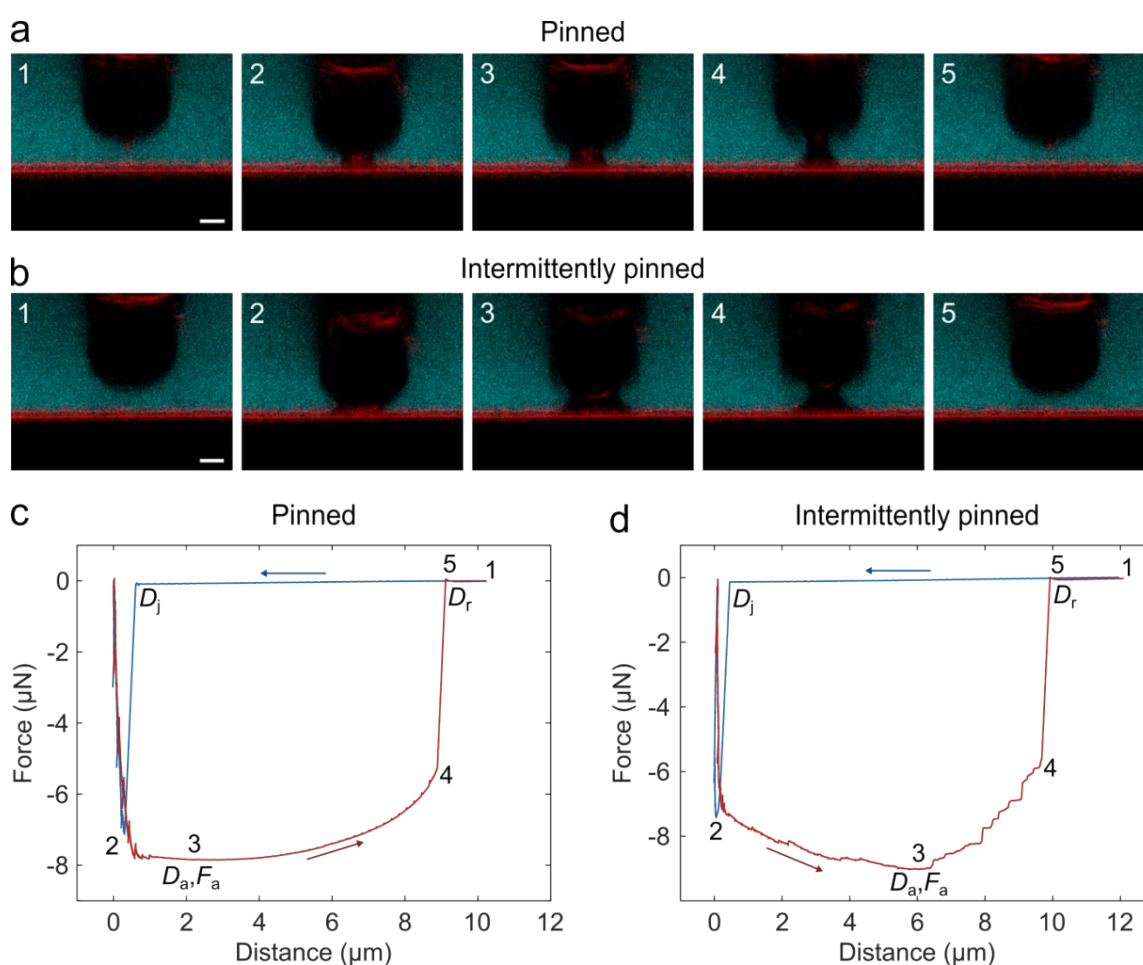

Figure 2. Top: Representative confocal images for (a) pinned and (b) intermittently pinned three-phase lines recorded at (1) the start of the measurement, (2) just after meniscus formation and jump-in, D_j, (3) at maximum attractive force, D_a (4) just before rupture, D_r, and (5) after rupture. Scale bar: 10 µm. Color code: Water in cyan and reflected light in red. Bottom: Force curves recorded in (a) and (b) are shown in (c) and (d), respectively.

The confocal images were analyzed (Supporting Information) to obtain the shape of the gas meniscus in order to determine the meniscus volume V_c, the meniscus diameter on the superhydrophobic surface d_c, the angle defining the de-wetted area on the hydrophobic particle β, the microscopic contact angles at the liquid-gas interface of the particle θ_p, and superhydrophobic surface θ_s (Figure 1c). Further, the pressure change across the liquid-gas interface Δp was calculated from the meniscus curvature (r_1 and r_2) and the surface tension of water (γ) using the Young-Laplace equation:

$$\Delta p = \gamma \left(\frac{1}{r_1} + \frac{1}{r_2} \right) \tag{1}$$

The value of r_1 was estimated by averaging the radii of the meniscus curvature of the two sides in the cross sectional xz image, and r_2 was estimated as the radius of the xy cross section at the narrowest point of the meniscus (Figure 1c). As r_1 describes the concave curvature of the gas meniscus it is defined as negative, while r_2 is positive since it describes the convex curvature.

The confocal images obtained during force measurements revealed the formation of a gas meniscus between the hydrophobic particle and the superhydrophobic surface (Figure 2 and Videos S1, S2, Supporting Information). As long as the particle and the superhydrophobic surface are well-separated, the force is zero (Figure 2, point 1). At some point below 1 µm separation, the surfaces jump into contact due to a strongly attractive force. The corresponding confocal images at the jump-in distance D_j demonstrate the formation of a gas meniscus (Figure 2, point 2). After the particle makes contact with the superhydrophobic surface at zero distance, the cantilever is retracted. The gas meniscus and the attractive force persist and reach a maximum force F_a at separation distance D_a (Figure 2, point 3). The gas meniscus can span distances up to 10 µm (Figure 2, point 4). The force returns back to zero when the meniscus ruptures at distance D_r (Figure 2, point 5).

Two types of local wetting were observed during separation. Most frequently (44 of 50 measurements), the meniscus was pinned to the superhydrophobic surface (Figure 2a and Video S1, Supporting Information). Its base diameter was constant during retraction until rupture. Less frequently (6 of 50 measurements), intermittent pinning to the surface was observed (Figure 2b and Video S2, Supporting Information). In this case the base diameter increased during separation. In a few additional cases, no gas meniscus was observed by confocal microscopy, likely because it was too small or that surface features prevented meniscus formation (Figure S4, Supporting Information). Force curves and confocal images were very reproducible for repeated measurements on the same spot (Figure S5, Supporting Information), suggesting that microscopic surface irregularities (topographical or chemical) determine the degree of pinning and local wetting properties.

Force curve characteristics for pinned and intermittently pinned three-phase lines show qualitative and quantitative differences (Table 1). For pinned contacts the force maximum on separation is reached at small distances, typically within the first 4 µm (Figure 3a). Upon further increase of distance, the force becomes less attractive and at around 9 µm the gas meniscus ruptures. These force curves are smooth. In contrast, for intermittent pinning the attractive force

first increases with increasing distance, reaches a maximum at around 6 µm and then decreases prior to rupture. In this case, many small steps are visible in the force curve and the maximum attraction is slightly stronger than for pinned contacts.

Table 1. Average values with standard deviations of the maximum attractive force (F_a), the jump-in distance (D_j), rupture distance (D_r) and the distance of maximum attraction (D_a) obtained from force measurements. The number of measurements is given in parentheses for each case.

	All measurements (50)	Pinned (44)	Intermittently pinned (6)
F_a (µN)	8.4 ± 0.5	8.3 ± 0.4	9.1 ± 0.2
D_j (µm)	0.5 ± 0.3	0.6 ± 0.3	0.3 ± 0.1
D_a (µm)	3.5 ± 1.9	3.1 ± 1.8	6.2 ± 0.1
D_r (µm)	9.4 ± 1.1	9.3 ± 1.1	10.0 ± 0.1

The volume of the gas meniscus increases with separation (Figure 3b), suggesting a transport of air from the layer at the superhydrophobic surface into the meniscus. Since the liquid was not de-gassed prior to measurements, it is possible that some gas will also enter the meniscus *via* diffusion from the bulk liquid. For pinned contacts the volume continues to increase beyond D_a due to elongation of the meniscus in *z*-direction with a nearly constant base diameter (Figure 3c). The contact angles on the superhydrophobic surface and on the particle increase moderately with surface separation (Figure 3d,e). Menisci with pinned three-phase lines are typically smaller (smaller values of d_c, β and r_2) than those with intermittently pinned three-phase lines both at the formation stage and during separation (Figure 3c,f,h). This suggests stronger hindrance to meniscus growth for the pinned case which is also reflected by maximum meniscus volume V_c being only 1/3 as compared to intermittently pinned situations (Figure 3b). The position β of the three-phase line on the particle is relatively constant until the maximum attractive force has been reached (Figure 3a,f). For $D > D_a$, β decreases as the three-phase line is moving over the surface of the particle (Figure 3f). This leads to a decrease in attractive force. We note that menisci having intermittently pinned three-phase lines reach their maximum volume at the distance where the attractive force is largest (Figure 3a,b). At larger distances the decreasing contact area of the meniscus on the particle explains the decreasing meniscus volume.
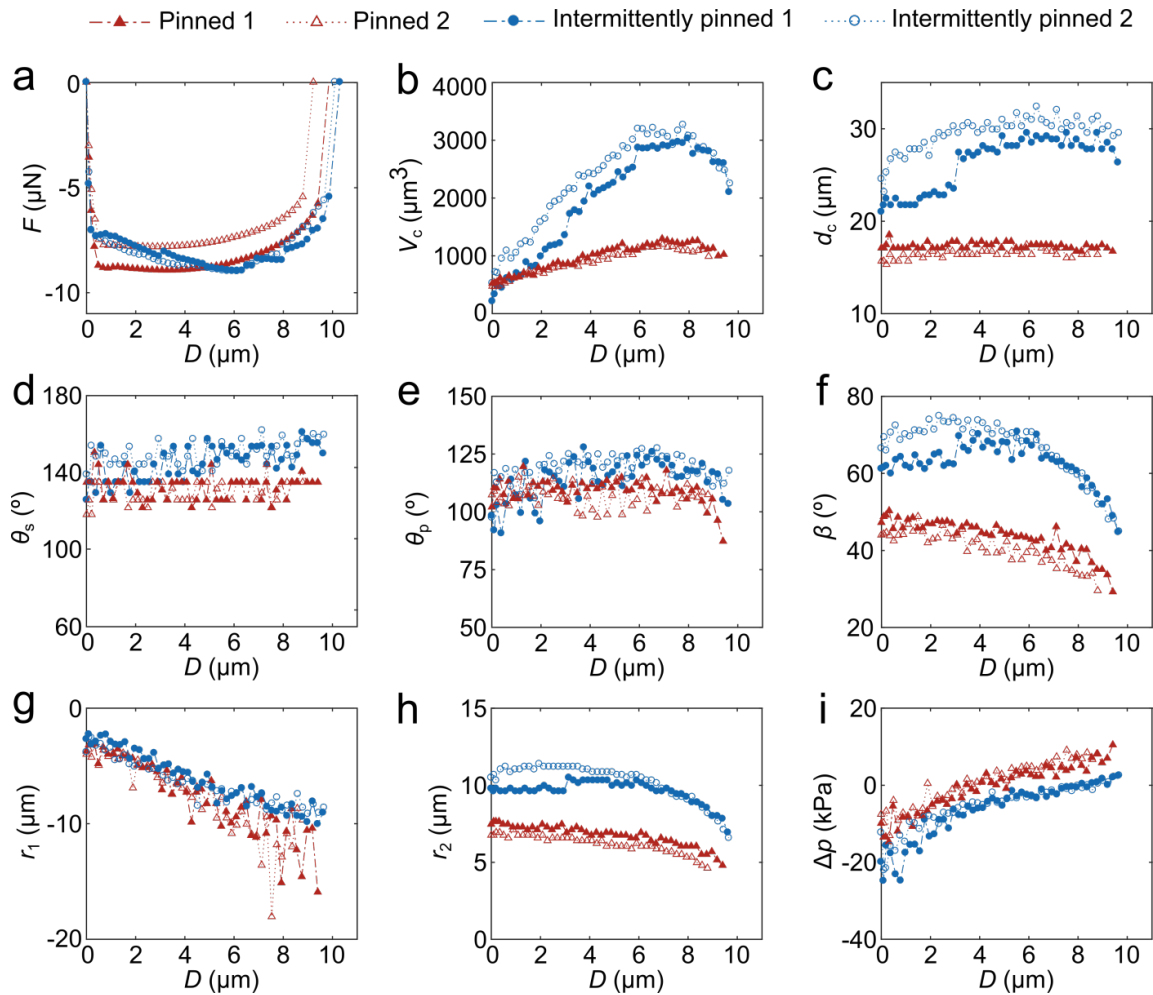
Figure 3. Plots of (a) force F (b) meniscus volume V_c , (c) base diameter at the superhydrophobic surface d_c, the microscopic contact angles at the liquid-gas interface of the (d) superhydrophobic surface θ_s and (e) hydrophobic particle θ_p, (f) angle defining the de-wetted area on the particle β, the two radii of the principal curvature of the liquid-gas interface (g) r_1 and (h) r_2 and (i) the pressure difference Δp as a function of separation distance D for two pinned (red triangles, open and closed symbols) and two intermittently pinned (blue circles) wetting cases recorded at different locations. The force in panel (a) was measured with colloidal probe AFM and the data in panels (b)-(i) were calculated from the size and shape of the gas meniscus determined from the confocal images.

The exact composition of the meniscus gaseous phase is not known, but determination of the pressure difference within the meniscus can provide information on whether it is derived mainly from trapped air or induced by water vaporization. The pressure difference is expressed as $\Delta p = p_v - p_l$, where p_v is the pressure inside the meniscus and p_l is the pressure in the liquid. In this case p_l is equal to atmospheric pressure ($\approx$ 100 kPa). If the meniscus contained only water vapor, p_v would be equal to the vapor pressure for water (3 kPa at 25 °C), and thus Δp would be close to

7

-100 kPa. Δp can be calculated from Eq. 1, using the principal radii of the curvature, r_1 and r_2 (Figure 1c). The calculated pressure drop over the meniscus interface is in the range of 0-20 kPa (Table 2). Thus, the meniscus needs to contain a large quantity of air. This is consistent with a pre-existing air layer at the rough superhydrophobic surface facilitating formation and growth of the gas meniscus. The under-pressure in the meniscus is the driving force for the gas flow from the air layer, and this allows the meniscus volume to increase (Figure 3b). The meniscus ruptures as soon as $\Delta p \approx 0$. Our data suggest a small overpressure exists in the meniscus prior to rupture (Table 2 and Figure 3i). This positive pressure could result from the onset of meniscus collapse, where gas need to be driven back from the meniscus into the air layer. However, for the very elongated, almost cylindrical shape of the meniscus before rupture, the radius r_1 is no longer well defined (Figure 3g) and this can lead to an increased uncertainty of pressure at rupture.

Table 2. Average values with standard deviation of meniscus characteristics obtained from confocal images at three specific points: jump-in distance (D_j), distance of maximum attraction (D_a), and rupture distance (D_r). The number of measurements is given in parentheses for each case.

	All measurements (50)			Pinned (44)			Intermittently pinned (6)		
	D_j	D_a	D_r	D_j	D_a	D_r	D_j	D_a	D_r
V_c (µm³)	340 ± 160	1060 ± 750	1140 ± 430	330 ± 170	800 ± 220	1000 ± 190	430 ± 100	2990 ± 200	2170 ± 220
d_c (µm)	19 ± 3	19 ± 4	18 ± 4	18 ± 3	18 ± 2	17 ± 2	23 ± 1	30 ± 1	28 ± 1
β (°)	52 ± 9	50 ± 8	35 ± 5	50 ± 8	47 ± 4	33 ± 4	66 ± 3	68 ± 4	44 ± 2
θ_s (°)	133 ± 13	134 ± 11	140 ± 9	132 ± 13	132 ± 10	138 ± 6	138 ± 7	150 ± 7	158 ± 7
θ_p (°)	98 ± 8	109 ± 7	105 ± 6	98 ± 8	107 ± 6	105 ± 6	98 ± 8	118 ± 6	108 ± 8
r_1 (µm)	-3.1 ± 1.2	-5.9 ± 1.8	-9.0 ± 1.6	-3.2 ± 1.2	-5.6 ± 1.7	-9.0 ± 1.6	-2.9 ± 0.9	-8.0 ± 0.7	-8.5 ± 1.0
r_2 (µm)	8.4 ± 1.3	7.8 ± 1.1	5.4 ± 0.8	8.1 ± 1.2	7.4 ± 0.5	5.3 ± 0.6	10.3 ± 0.3	10.3 ± 0.5	6.8 ± 0.2
Δp (kPa)	-18 ± 14	-4 ± 4	5 ± 3	-18 ± 14	-4 ± 4	6 ± 3	-19 ± 8	-2 ± 1	2 ± 1

The attractive force (F_a) between a sphere and a plane in a non-wetting liquid can be expressed as the sum of two contributions [33]:

$$F_a = F_{\Delta p} + F_\gamma \tag{2}$$

The first term ($F_{\Delta p}$) arises from the pressure difference across the liquid-gas interface and is given by

$$F_{\Delta p} = \frac{1}{4}\pi d_c^2 \Delta p \tag{3}$$

The second term (F_γ) is due to the surface tension acting on the wetted perimeter, and is given by

$$F_\gamma = -\pi d_c \gamma \sin\theta_s \tag{4}$$

The adhesion in the saturated vapor will theoretically also contribute, but adsorption of a non-wetting liquid is assumed to be insignificant and is neglected. The values for d_c, θ_s and Δp were estimated from the confocal images at the distance D_a and calculations give $F_a = -4.1 \pm 1.0\ \mu N$. When calculating F_a for the two wetting cases separately, we get $F_a = -4.0 \pm 1.0\ \mu N$ and $F_a = -4.9 \pm 0.9\ \mu N$ for pinned and intermittently pinned three-phase lines, respectively. These values are in the same order of magnitude as the data obtained from force measurements (average $F_a = -8.4 \pm 0.5\ \mu N$, Table 1). Thus, when the gas meniscus spreads on the surface, creating a larger non-wetted area, the maximum attractive force increases.

Stepwise reduction of the attractive force was observed for the intermittently pinned wetting case. When these steps occur at distances smaller than D_a, we relate the changes in F to a decrease in Δp as additional gas from the air layer enters the meniscus. In some cases this small pressure change is caused by a moving three-phase line on either the superhydrophobic surface (change in d_c) or hydrophobic particle (change in β) (Figure S6, Supporting Information). We can estimate the change in under-pressure, $\Delta(\Delta p)$, from the steps in the force curve. If d_c is constant, F_γ will be constant (Eq. 4) and the change in force ΔF can be expressed as

$$\Delta F = \frac{1}{4}\pi d_c^2 \Delta(\Delta p) \tag{5}$$

The steps from the recorded force curves are in the order of $\Delta F = 0.2\ \mu N$, and the meniscus diameter is typically $25\text{-}30\ \mu m$, giving $\Delta(\Delta p) = 0.3\text{-}0.4\ kPa$. These changes are, however, too small to be directly seen in the data calculated from the confocal images (Figure 3i).

The rupture distance can be estimated from a free energy balance. Realizing that at D_r the free energy for the de-wetted and wetted situation is equal we arrive at the following equation, where ΔG is the free energy difference between the de-wetted and the wetted states:

$$\Delta G = \Delta G_p + \Delta G_s + \Delta G_i + \Delta G_c = A_p\gamma\cos\theta_p + A_s\gamma\cos\theta_s + A_i\gamma - V_c\Delta p = 0 \tag{6}$$

Here, A_p and A_s are the de-wetted areas on the particle and the superhydrophobic surface, respectively. The area of the meniscus gas-water interface A_i is given by $A_i = 2\pi\int_0^D rdD$, where r is the meniscus radius at each point between the particle and superhydrophobic surface and D the distance between the two surfaces. Since our data show that $\Delta p \approx 0$ at rupture it is justified to ignore the last term. By using the local contact angles (Table 2) and calculating the interfacial areas from d_c, β and the area of the gas-water interface as estimated from the image of the meniscus (Supporting Information) we calculate D_r to about $11\ \mu m$, which is close to our experimental value (average $D_r = 9.4 \pm 1.1\ \mu m$, Table 1).

CONCLUSIONS

Gas meniscus formation was monitored with confocal microscopy during force measurements between a superhydrophobic surface and a hydrophobic microsphere in water. The confocal images allowed us to determine the meniscus volume and shape. Forces calculated from the meniscus size and shape are consistent with the forces measured using colloidal probe AFM. We

conclude that the pre-existing air layer at the superhydrophobic surface facilitates the formation and growth of the meniscus. The under-pressure in the meniscus is the driving force for gas flow from the air layer into the meniscus.

METHODS

Sample preparation. Superhydrophobic coatings were prepared on high precision thin cover glasses (No. 1.5H, thickness 170±5 µm, Carl Roth GmbH). The glass substrates were rinsed in Milli-Q water and ethanol, dried under N_2 and plasma cleaned using a table top plasma cleaner (PDC-32G, Harrick Plasma) for 1 min at 18 W prior to the coating procedure. To induce the required surface roughness, the substrates were dip coated three times in a formulation consisting of 0.5 wt% silica nanoparticles (Aerosil R972, Degussa AG) dispersed in 87 wt% hydrofluoroether (HFE 7100, 3M) and 12.5 wt% perfluoroalkyl copolymer (FluoroPEL™ PFC 604A, Cytonix Corporation). To make the particle coating more durable the coated samples were heat treated at 450 °C for 2 h. Finally, the samples were silanized with 1H,1H,2H,2H-perfluorooctyltrietoxysilane (ABCR GmbH & Co. KG) in gas phase in a N_2 atmosphere at 70 °C for 24 h.

Glass microspheres (diameter 10-40 µm, Polysciences Inc.) were glued to tipless cantilevers (NSC35/tipless/Cr-Au, Mikromasch) by a small amount of two-component glue (Epoxy Rapid, Bostik) using a micromanipulator under an optical microscope. The particles were hydrophobized by gas phase silanization as described above for the superhydrophobic surface. Cantilevers were calibrated using the method described by Sader.[34]

Surface characterization. AFM topography images for roughness analysis of the superhydrophobic surfaces and hydrophobic particle were recorded with a Bruker Multimode 8 AFM with Nanoscope V Controller (Bruker) using silicon nitride cantilevers (ScanAsyst Air, Bruker) with typical spring constant of 0.4 Nm^{-1}.

Water contact angle measurements were performed using a DataPhysics OCA40 micro system (DataPhysics GmbH). A 5 µL Milli-Q purified water droplet was gently deposited on the surface and the contact angle and roll-off angle were measured. The advancing and receding contact angles were determined when the droplet started to roll. All contact angles were determined using the tangent fitting method and the results of 10 individual measurements at different locations on the sample were averaged.

Laser scanning confocal microscopy combined with colloidal probe AFM. A specially designed inverted laser scanning confocal microscope set-up[31-32] coupled with a JPK NanoWizard AFM (JPK Instruments AG) was used for confocal imaging during force measurements. The confocal microscope used a 40x/N.A.=0.95 dry objective with a correction ring and a 473 nm laser (Cobolt blue 25 mW). MilliQ purified water with a fluorescent dye (Atto 488, Atto-tec GmbH) added at a concentration of 10 mg L^{-1} was used in the experiments. The fluorescence from the dyed water and the reflected light from the interfaces were detected simultaneously with two different detectors. The microscope was operated in *xz*-mode in which the laser was scanned along one line in the *x* direction at different heights in the *z* direction to render a 2D cross-sectional

image. An average of 16 line scans was used to give the final image. Confocal images were taken at an acquisition rate of 1 frame s^{-1} and the AFM head was moving with a constant speed of 0.2 µm s^{-1} during approach and retraction.

ASSOCIATED CONTENT

Supporting Information. The following files are available free of charge.

Video with confocal images of a gas meniscus pinned to the superhydrophobic surface during separation (AVI)

Video with confocal images of a gas meniscus intermittently pinned to the superhydrophobic surface during separation (AVI)

Surface tension of water with Atto 488, image analysis, calculations of meniscus interfacial areas, AFM topography image hydrophobic particle, molecular structure Atto 488, confocal microscopy images, repeated force curves and force curve with less long-ranged interactions (PDF)

AUTHOR INFORMATION

Corresponding Authors

* E-mail: mimmi.eriksson@ri.se. * E-mail: teisala@mpip-mainz.mpg.de.

REFERENCES

1. Israelachvili, J.; Pashley, R., The Hydrophobic Interaction Is Long Range, Decaying Exponentially with Distance. *Nature* **1982,** *300*, 341-342.

2.   Lohse, D.; Zhang, X., Surface Nanobubbles and Nanodroplets. *Rev. Mod. Phys.* **2015,** *87*, 981-1035.

3.   Israelachvili, J. N.; Pashley, R. M., Measurement of the Hydrophobic Interactionbetween Two Hydrophobic Surfaces in Aqueous Electrolyte Solutions. *J. Colloid Interface Sci.* **1984,** *98*, 500-514.

4.   Parker, J. L.; Claesson, P. M., Direct Measurements of the Attraction between Solvophobic Surfaces in Ethylene Glycol and Mixtures with Water. *Langmuir* **1992,** *8*, 757-759.

5.   Parker, J. L.; Claesson, P. M.; Attard, P., Bubbles, Cavities, and The Long-Ranged Attraction between Hydrophobic Surfaces. *J. Phys. Chem.* **1994,** *98*, 8468-8480.

6.   Carambassis, A.; Jonker, L. C.; Attard, P.; Rutland, M. W., Forces Measured between Hydrophobic Surfaces Due to a Submicroscopic Bridging Bubble. *Phys. Rev. Lett.* **1998,** *80*, 5357-5360.

7.   Christenson, H. K.; Claesson, P. M., Direct Measurements of the Force between Hydrophobic Surfaces in Water. *Adv. Colloid Interface Sci.* **2001,** *91*, 391-436.

8.   Thormann, E.; Simonsen, A. C.; Hansen, P. L.; Mouritsen, O. G., Force Trace Hysteresis and Temperature Dependence of Bridging Nanobubble Induced Forces between Hydrophobic Surfaces. *ACS Nano* **2008,** *2*, 1817-1824.

9.   Azadi, M.; Nguyen, A. V.; Yakubov, G. E., Attractive Forces between Hydrophobic Solid Surfaces Measured by AFM on the First Approach in Salt Solutions and in the Presence of Dissolved Gases. *Langmuir* **2015,** *31*, 1941-1949.

10.   Kanduč, M.; Netz, R. R., From Hydration Repulsion to Dry Adhesion between Asymmetric Hydrophilic and Hydrophobic Surfaces. *Proc. Natl. Acad. Sci. U.S.A.* **2015,** *112*, 12338-12343.

11.   Donaldson, S. H.; Røyne, A.; Kristiansen, K.; Rapp, M. V.; Das, S.; Gebbie, M. A.; Lee, D. W.; Stock, P.; Valtiner, M.; Israelachvili, J., Developing a General Interaction Potential For Hydrophobic and Hydrophilic Interactions. *Langmuir* **2015,** *31*, 2051-2064.

12.   Ishida, N.; Matsuo, K.; Imamura, K.; Craig, V. S. J., Hydrophobic Attraction Measured between Asymmetric Hydrophobic Surfaces. *Langmuir* **2018,** *34*, 3588-3596.

13.   Mastropietro, D. J.; Ducker, W. A., Forces between Hydrophobic Solids in Concentrated Aqueous Salt Solution. *Phys. Rev. Lett.* **2012,** *108*, 106101.

14.   Ishida, N.; Sakamoto, M.; Miyahara, M.; Higashitani, K., Optical Observation of Gas Bridging between Hydrophobic Surfaces in Water. *J. Colloid Interface Sci.* **2002,** *253*, 112-116.

15.   Christenson, H. K.; Claesson, P. M., Cavitation and the Interaction between Macroscopic Hydrophobic Surfaces. *Science* **1988,** *239*, 390-392.

16.   Barthlott, W.; Neinhuis, C., Purity of the Sacred Lotus, or Escape from Contamination in Biological Surfaces. *Planta* **1997,** *202*, 1-8.

17.   Neinhuis, C.; Barthlott, W., Characterization and Distribution of Water-Repellent, Self-Cleaning Plant Surfaces. *Ann. Bot.* **1997,** *79*, 667-677.

18. Wenzel, R. N., Resistance of Solid Surfaces to Wetting by Water. *Ind. Eng. Chem.* **1936,** *28*, 988-994.

19. Cassie, A. B. D.; Baxter, S., Wettability of Porous Surfaces. *Trans. Faraday Society* **1944,** *40*, 546-551.

20. Luo, C.; Xiang, M.; Heng, X., A Stable Intermediate Wetting State after a Water Drop Contacts the Bottom of a Microchannel or Is Placed on a Single Corner. *Langmuir* **2012,** *28*, 9554-9561.

21. Verho, T.; Korhonen, J. T.; Sainiemi, L.; Jokinen, V.; Bower, C.; Franze, K.; Franssila, S.; Andrew, P.; Ikkala, O.; Ras, R. H. A., Reversible Switching between Superhydrophobic States on a Hierarchically Structured Surface. *Proc. Natl. Acad. Sci. U.S.A.* **2012,** *109*, 10210-10213.

22. Singh, S.; Houston, J.; van Swol, F.; Brinker, C. J., Superhydrophobicity: Drying Transition of Confined Water. *Nature* **2006,** *442*, 526-526.

23. Hansson, P. M.; Swerin, A.; Schoelkopf, J.; Gane, P. A. C.; Thormann, E., Influence of Surface Topography on the Interactions between Nanostructured Hydrophobic Surfaces. *Langmuir* **2012,** *28*, 8026-8034.

24. Wåhlander, M.; Hansson-Mille, P. M.; Swerin, A., Superhydrophobicity: Cavity Growth and Wetting Transition. *J. Colloid Interface Sci.* **2015,** *448*, 482-491.

25. Thormann, E., Surface Forces between Rough and Topographically Structured Interfaces. *Curr. Opin. Colloid Interface Sci.* **2017,** *27*, 18-24.

26. Papadopoulos, P.; Deng, X.; Mammen, L.; Drotlef, D.-M.; Battagliarin, G.; Li, C.; Müllen, K.; Landfester, K.; del Campo, A.; Butt, H.-J.; Vollmer, D., Wetting on the Microscale: Shape of a Liquid Drop on a Microstructured Surface at Different Length Scales. *Langmuir* **2012,** *28*, 8392-8398.

27. Luo, C.; Zheng, H.; Wang, L.; Fang, H.; Hu, J.; Fan, C.; Cao, Y.; Wang, J., Direct Three-Dimensional Imaging of the Buried Interfaces between Water and Superhydrophobic Surfaces. *Angew. Chem. Int. Ed. Engl.* **2010,** *49*, 9145-9148.

28. Papadopoulos, P.; Mammen, L.; Deng, X.; Vollmer, D.; Butt, H.-J., How Superhydrophobicity Breaks Down. *Proc. Natl. Acad. Sci. U.S.A.* **2013,** *110*, 3254-3258.

29. Lv, P.; Xue, Y.; Shi, Y.; Lin, H.; Duan, H., Metastable States and Wetting Transition of Submerged Superhydrophobic Structures. *Phys. Rev. Lett.* **2014,** *112*, 196101.

30. Schellenberger, F.; Encinas, N.; Vollmer, D.; Butt, H.-J., How Water Advances on Superhydrophobic Surfaces. *Phys. Rev. Lett.* **2016,** *116*, 096101.

31. Schellenberger, F.; Papadopoulos, P.; Kappl, M.; Weber, S. A. L.; Vollmer, D.; Butt, H.-J., Detaching Microparticles from a Liquid Surface. *Phys. Rev. Lett.* **2018,** *121*, 048002.

32. Pham, J. T.; Schellenberger, F.; Kappl, M.; Butt, H.-J., From Elasticity to Capillarity in Soft Materials Indentation. *Phys. Rev. Mater.* **2017,** *1*, 015602.

33. Yaminsky, V. V.; Yushchenko, V. S.; Amelina, E. A.; Shchukin, E. D., Cavity Formation Due to a Contact between Particles in a Nonwetting Liquid. *J. Colloid Interface Sci.* **1983,** *96*, 301-306.

34. Sader, J. E.; Chon, J. W. M.; Mulvaney, P., Calibration of Rectangular Atomic Force Microscope Cantilevers. *Rev. Sci. Instrum.* **1999,** *70*, 3967-3969.

35. Heydari, G.; Thormann, E.; Järn, M.; Tyrode, E.; Claesson, P. M., Hydrophobic Surfaces: Topography Effects on Wetting by Supercooled Water and Freezing Delay. *J. Phys. Chem. C* **2013,** *117*, 21752-21762.

For Table of Contents Only: